Atmospheric Environment 186 (2018) 45–55

Contents lists available at ScienceDirect

Atmospheric Environment

journal homepage: www.elsevier.com/locate/atmosenv

Observational evidence for direct uptake of ozone in China by Asian dust in springtime

Yang Nan[a], Yuxuan Wang[a,b,*]

[a] Department of Earth System Science, Tsinghua University, Beijing, China
[b] Department of Earth & Atmospheric Sciences, University of Houston, Houston, TX, United States

ARTICLE INFO

Keywords:
Asian dust
O_3
Uptake
China
Surface observations

Abstract: While there is ample observational evidence for ozone uptake by Sahara dust, whether Asian dust exerts a similar effect on ozone has not been well-established in the literature due in part to limited observations. In this study we investigate the impacts of Asian dust on surface ozone (O_3) over northern China on a daily scale using observations from recently established air quality monitoring network during spring (March, April, May; MAM) 2015–2017, the peak season of Asian dust outbreaks. Dust days and non-dust days are selected based on the distribution of the coarse-mode particulate matter mass concentrations (PM_{coarse}) and then paired based on similar temperature (T) and relative humidity (RH) so as to minimize the effect of different local meteorological conditions on ozone. The majority of the dust days shows lower O_3 compared to non-dust days both temporally and spatially. The regional average of seasonal-mean O_3 differences between dust days and their reference non-day days are −10.1 ppbv (−24.6%), −2.4 ppbv (−4.8%) and −5.4 ppbv (−14.3%) over the Taklimakan Desert (TD), the Gobi Desert (GD) and North China (NC), respectively. The decrease of ozone tends to increase with increasing PM_{coarse}, although the use of PM_{coarse} to indicate dust is subject to uncertainty. Nitrogen dioxide (NO_2), sulfate dioxide (SO_2), and carbon monoxide (CO) appear to be higher during dust days outside dust source regions, possibly because of the compounding effects of large anthropogenic emissions over this region. In spite of higher or similar levels of primary pollutants, surface ozone concentrations are still lower during dust days over TD, GD and NC, supporting the mechanism of dust direct uptake of O_3.

1. Introduction

Mineral dust is the largest contributor of aerosols in the atmosphere. It is estimated that about 500–6000 Tg of dust aerosols are mobilized globally from arid or semiarid regions annually by strong winds and entrained into the atmosphere (Ginoux et al., 2001; Zender et al., 2003). The largest contributions to global dust loading are from the North African (50–70%) and Asian deserts (10–25%) (Tegen and Schepanski, 2009). Major dust sources in East Asia are the Taklimakan Desert in northwestern China, and the Gobi Desert over northern China and Mongolia. Dust storms over East Asia occur primarily in springtime, and suspended dust aerosols in the atmosphere can be transported long distances to the northern Pacific and even globally (Uno et al., 2009), affecting air quality (Yang et al., 2017), hydrological cycle (Rosenfeld et al., 2001; Shao et al., 2011), and regional climate (Huang et al., 2015). For example, a dust storm affected the Beijing metropolitan area on 15 April 2015 with surface hourly PM_{10} (particulate matter smaller than 10 μm in diameter) reaching more than 1000 μg/m^3 (http://www.chinadaily.com.cn/beijing/2015-04/16/content_20450286.htm). Under such high dust levels, the interactions of mineral dust with gases and other aerosol particulates in the atmosphere are expected to be complex and need to be understood.

One important aspect of mineral dust on atmospheric chemistry is uptake of gaseous species. For example, low ozone (O_3) mixing ratios have been measured concurrently with dust events. Bonasoni et al. (2004) reported that ozone mixing ratios were 4%–21% lower than the monthly mean background values during Saharan dust events in the Mediterranean region. Andrey et al. (2014) found systematically lower ozone mixing ratios during Saharan air layer days (SAL) than those during clean conditions, and the difference reached up to −35% based on 157 ozonesonde profiles launched from the Canary Islands over 13 summers. Jenkins et al. (2012) found a 20–30 ppbv decrease of ozone in some cases between SAL and non-SAL conditions in the Eastern Atlantic during the summer of 2010. Soler et al. (2016) recorded an average ozone reduction of 5.5% during Saharan events at a mountain station located near the eastern coast of the Iberian Peninsula from May to September 2012.

Three pathways have been proposed to explain the observed O_3

* Corresponding author. Department of Earth System Science, Tsinghua University, Beijing, China.
E-mail address: ywang246@central.uh.edu (Y. Wang).

https://doi.org/10.1016/j.atmosenv.2018.05.032
Received 2 December 2017; Received in revised form 15 April 2018; Accepted 14 May 2018
Available online 15 May 2018
1352-2310/

reductions during dust events: (1) a decrease in net production rate of ozone due to the effect of dust on the transmissivity of solar radiation in the atmosphere; (2) the direct uptake of O_3 by dust; and (3) dust uptake of ozone precursors (e.g. nitrogen oxides). The latter two pathways involve heterogeneous reactions on dust. The uptake of O_3 on clean dust surface was found to be catalytic, and under dry conditions, the reactive sites were thought to be Lewis acid sites (Usher et al., 2003). Nitrogen oxides, as precursors of O_3, have a strong tendency to react with alkaline dust aerosols, forming water-soluble aerosols like calcium nitrate (Usher et al., 2003). Because of complex mechanisms and scarcity of direct field measurements, rates of ozone reduction as a function of dust loading have been primarily inferred from laboratory measurements (Crowley et al., 2010; Goodman et al., 2001; Hanisch and Crowley, 2003; Johnson et al., 2005; Michel et al., 2002; Underwood et al., 2001; Usher et al., 2002).

Based on laboratory information, modeling studies have assessed the impacts of dust on O_3, using laboratory-derived "best guess" of uptake coefficients of ozone and precursor gases on dust. The majority of published modeling studies, as listed below, suggest that light scattering by dust particles leads to a decrease of direct radiation but an increase of diffusive radiation in the lower atmosphere, and the combined radiative effect by dust is small for photolysis rate calculation. Therefore, heterogeneous reactions likely play the dominant role in the overall effects of dust on O_3. Reus et al. (2000) estimated a heterogeneous O_3 loss of 4 ppbv per day (half from nitrogen oxides uptake and the other half from O_3 uptake) near Tenerife, Canary Islands, in July 1997, compared to an estimated O_3 loss of 0.2 ppbv per day from low photolysis rate. Liao et al. (2003) included aerosols in their photolysis calculation and found the effect to be less than 0.2 ppbv reduction of monthly mean O_3. Bian and Zender (2003) showed that O_3 globally increased about 0.2% in the annual mean due to the impact of mineral dust on photolysis rates. Tang et al. (2004) simulated an O_3 decrease of about 20 ppbv as a result of heterogeneous reactions on dust in Asian dust outflow, compared to less than 1 ppbv decrease due to dust radiative influence. Bauer et al. (2004) suggested a decrease in global tropospheric ozone mass by about 5.4% due to heterogeneous reactions on dust, including 4.9% from nitrogen oxides uptakes and only 0.5% from O_3 uptake. Pozzoli et al. (2008) showed that heterogeneous reactions on dust would reduce ozone surface concentrations by 18–23% over the Asian outflow region and the global annual mean O_3 burden by 7%. Wang et al. (2012) estimated O_3 reductions of up to 3.8 ppb (~9%) by heterogeneous reactions on dust during the April 2001 dust storm episode over the trans-Pacific domain. These model simulations with heterogeneous reactions tend to have a better agreement with field observations.

Most of the field evidence in support of the modeling calculations was based on African dust events, although laboratory studies suggest both Asian and African dust uptake ozone and other gases. There were fewer direct field observations of Asian dust, and previous analysis of them had contradictory conclusions. Tang et al. (2004) showed lower O_3 mixing ratio during one Asian dust outflow episode during an aircraft campaign over the Yellow Sea in spring 2001. Fairlie et al. (2010) did not detect O_3 depletion in Asian dust plumes encountered during another aircraft campaign during spring 2006 over the northeast Pacific. The contradiction might be due to the fact that these aircraft campaigns were snap-shots of atmospheric composition a few hundred to thousand kilometers downwind of Asia, where suspended dust particle concentrations were much less than those near dust sources. Meteorological conditions can significantly affect ozone daily variability and may even dominate the dust effect. Furthermore, the properties of Asian dust particles may have been significantly influenced by anthropogenic air pollutants during their transport across polluted eastern China.

To assess the effects of Asian dust on ozone, we examine the dust-ozone relationship within or close to the source regions, using daily surface air quality observations in China along the dust transport route from the Taklimakan Desert (TD) in the west and the Gobi Desert (GD) in the central, to North China (NC) in the east. The rest of the paper is organized as follows. Section 2 describes the data source and study domain. Here daily observations of surface particulate matters (PM), ozone, and meteorological conditions during March, April, and May (MAM) are used to analyze the covariance between dust and ozone from 2015 to 2017, with a focus on 2015. Section 3 summarizes daily variations of springtime PM and O_3 in three representative regions over northern China. Due to the lack of dust observations, coarse particulate matter mass concentration (PM_{coarse}) is chosen as an indicator of dust and we verify this indicator with reported dust episodes. Section 4 demonstrates the significant meteorological effects on day-to-day O_3 variability. Section 5 investigates the differences of O_3 between dust and non-dust days, after the influences of meteorological factors are taken into consideration. In section 6, we discuss comparisons to previous field studies, mechanisms and limitations. Section 7 gives final conclusions.

2. Data and study domains

2.1. Surface air quality and meteorological observations

Hourly concentrations of $PM_{2.5}$ (particulate matter less than 2.5 μm in diameter), PM_{10}, O_3, nitrogen dioxide (NO_2), sulfate dioxide (SO_2) and carbon monoxide (CO) at 1497 surface sites in China were obtained from the China Ministry of Ecology and Environment (MEE). This dataset was made available to the public in 2013, and here we focus on the springtime (March, April, May; MAM) from 2015 to 2017. PM_{coarse} was calculated by subtracting $PM_{2.5}$ from PM_{10}. The original unit of these MEE observations is μg/m^3. For O_3, NO_2, SO_2, and CO, we converted them to mixing ratios (units: ppmv for CO and ppbv for the rest) using a constant temperature of 298 K and atmospheric pressure of 1013.25 hPa. The site-level data were averaged into horizontal grids of 0.25° × 0.25° resolution to reduce sampling differences between nearby sites and to match with the resolution of meteorological reanalysis data. Daily gridded observations were derived using the hourly gridded data. For simplicity, the observational analysis of the 2015 springtime data is presented below. Similar analyses of the 2016 and 2017 spring data are shown in the supplementary material.

To analyze the influence of meteorology on surface O_3 variability, we obtained 2 m temperature (T), 2 m dew point temperature, 10 m zonal (U) and meridional (V) wind component, mean sea-level pressure, surface net solar radiation, boundary layer height, and total precipitation from the European Centre for Medium-Range Weather Forecasts (ECMWF) Reanalysis Interim (ERA-Interim) at a horizontal resolution of 0.25° × 0.25°. The 2 m relative humidity (RH) is then derived from the 2 m dew point. The 10 m wind speed is calculated as the square root of total squares of U and V.

2.2. Study domains

Fig. 1 presents China's land use and land cover categories in 2010 (Zhang et al., 2014) and the distribution of MAM-mean surface $PM_{2.5}$ and PM_{10} in 2015. There are two major dust source regions in northwestern China (Fig. 1a): the Taklimakan Desert (TD; 75°–87.5° E, 36°–43° N) and the Gobi Desert (GD; 95°–110° E, 35°-41°N). As the prevailing transport routes of dust from TD and GD are eastwards in springtime, the populous, and economically important region of North China (NC, 110°–120° E, 35°–41° N) is chosen as the major downwind and receptor region of dust storms from TD and GD (Sun et al., 2001).

In spring, the high PM_{10} concentrations in northern China were found to be associated with the occurrence of dust events (Feng et al., 2011). Indeed, surface PM_{10} concentrations (Fig. 1b) show a clear west-to-east gradient, decreasing from the seasonal average of more than 300 μg/m^3 over TD to 100–125 μg/m^3 over GD and NC, consistent with the west-to-east transport pathway of dust. By comparison, PM_{10} in

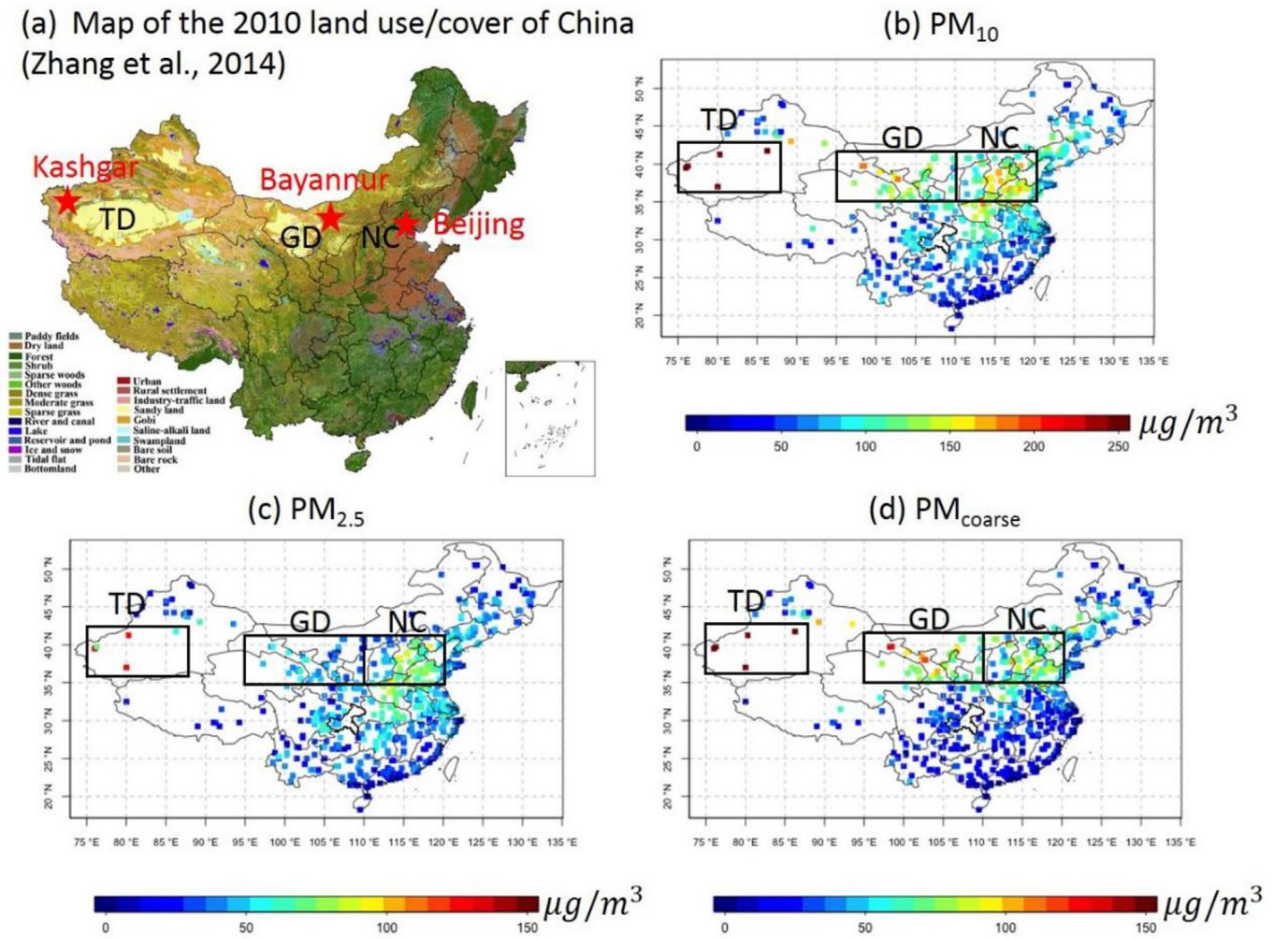

Fig. 1. Map of the 2010 land use/cover of China (Zhang et al., 2014) (a). Seasonal-mean daily concentrations of 0.25° × 0.25° gridded MEE surface PM_{10} (b), $PM_{2.5}$ (c), and PM_{coarse} (d) over China during spring 2015. The Taklimakan Desert (TD, 75°–87.5° E, 36°–43° N), the Gobi Desert (GD, 95°–110° E, 35°–41° N) and North China (NC, 110°–120° E, 35°–41° N) are shown in black rectangles from west to east over northern China. Red stars in Fig. 1a are three representative cities: Kashgar in TD, Bayannur in GD and Beijing in NC. (For interpretation of the references to colour in this figure legend, the reader is referred to the Web version of this article.)

other regions is lower than TD, GD and NC, indicating mineral dust is a major component of PM_{10} over these regions. $PM_{2.5}$ shows a similar west-to-east but smaller gradient, decreasing from about 100 μg/m^3 over TD to about 50 μg/m^3 over NC (Fig. 1c). In addition to mineral dust, anthropogenic aerosols are major components of $PM_{2.5}$ over NC (Wang et al., 2015; Zhang et al., 2015). NO_2, SO_2 and CO are emitted mainly from anthropogenic activities over China (Zhang et al., 2009). Regional-mean concentrations of NO_2, SO_2 and CO over both TD and GD are much lower (−17.1 ~ -44.4%) than those over NC (Table S1), indicating that anthropogenic emissions over TD and GD are much less than those over NC.

3. Daily variations of springtime surface PM and O_3 in three representative cities

To examine the dust effects on day-to-day variability of surface ozone, we first examine the relationship between ozone and dust by analyzing the time series of MEE observations. Here we use PM_{coarse} as an indicator of dust influences because we do not have observations of mineral dust with good temporal and spatial coverage in China. All the MEE stations provide parallel PM_{10} and $PM_{2.5}$ measurements. Dust aerosols have a size range and may be present in both $PM_{2.5}$ and PM_{10} (Kok, 2011). By contrast, anthropogenic aerosols (except fugitive dust) mainly reside in $PM_{2.5}$ (Donkelaar et al., 2010). Abundant evidence from field observations suggests that secondary aerosols formed from precursor gases are the dominant component of surface $PM_{2.5}$ in China (Guo et al., 2014; Wang et al., 2015, 2016). Therefore, PM_{coarse} is expected to consist of coarse-mode dust, including both mineral dust and fugitive dust, with minimal influences of anthropogenic aerosols. As fine-mode dust will not be represented in PM_{coarse}, this indicator underestimates dust mass concentrations. However, as we expect fine-mode dust to co-occur with coarse-mode dust during major dust episodes, PM_{coarse} would be a good indicator of the timing of dust events. Fig. 1d represents MAM-mean PM_{coarse} at the surface. Similar to $PM_{2.5}$ and PM_{10}, there is a west-to-east gradient in PM_{coarse}, with its concentration decreasing from more than 150 μg/m^3 over TD to about 50 μg/m^3 over GD and NC. There are clear boundaries of PM_{coarse} between the three defined regions (i.e. TD, GD, and NC) and the other regions. Using PM_{coarse} instead of PM_{10} or $PM_{2.5}$, these regions along the dust transport route (TD, GD and NC) are more distinguishable from other regions.

To illustrate the approach of using daily variability of PM_{coarse} to detect dust outbreaks, we show in Fig. 2 time series of daily surface concentrations of O_3, PM_{10}, $PM_{2.5}$ and PM_{coarse} during MAM 2015 at three representative cities, one from each region: Kashgar in TD (a), Bayannur in GD (b) and Beijing in NC (c). Fig. 2 also labels the days of known, large, dust outbreaks (D1-D10) from public news and published field studies (Lv et al., 2015; Wang et al., 2017). Over Kashgar in TD,

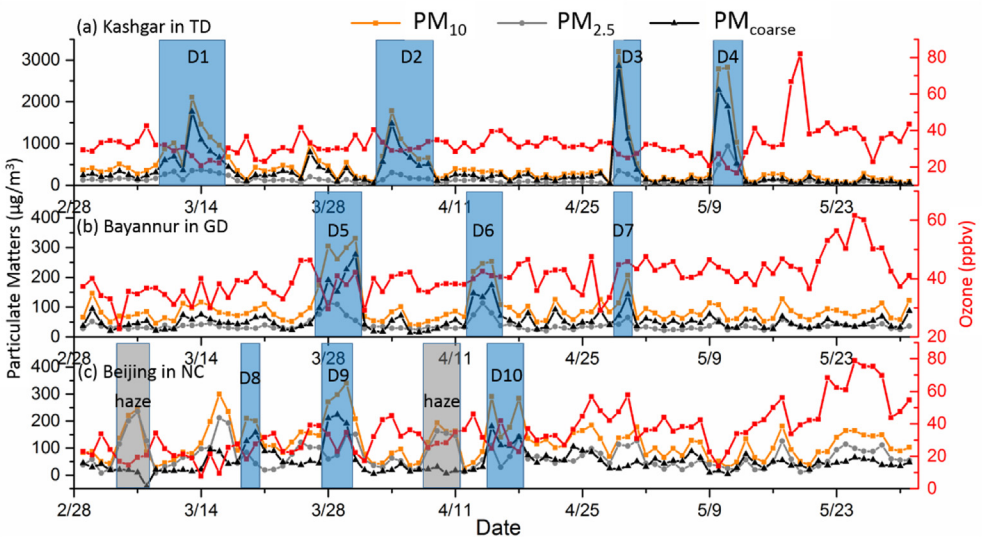

Fig. 2. Time series of daily concentrations of PM_{10}, $PM_{2.5}$, PM_{coarse}, and O_3 over Kashgar (a) in TD, Bayannur (b) in GD, and Beijing (c) in NC during spring 2015. The black, orange, gray and red lines are for PM_{coarse}, PM_{10}, $PM_{2.5}$, and O_3, respectively. The blue (i.e. D1-D10) and gray rectangles are shown for dust outbreaks and haze days. (For interpretation of the references to colour in this figure legend, the reader is referred to the Web version of this article.)

mass concentrations of PM_{10} are less than 500 μg/m^3 outside the dust outbreak days. PM_{10} and PM_{coarse} increased to more than 1000 μg/m^3 during D1-D4, reaching up to 3200 μg/m^3 and 2856 μg/m^3 on 29 April (Fig. 2a). Over Bayannur in GD, concentrations of PM_{10} and $PM_{2.5}$ are typically less than 100 μg/m^3. PM_{10} and PM_{coarse} increase to more than 250 μg/m^3 during dust episodes D5-D7 (Fig. 2b). Over Beijing in NC, the mean concentration of PM_{coarse} during the dust episodes (D8-D10) is 161 μg/m^3 was three times the corresponding seasonal mean. For Beijing, it is more difficult to distinguish the dust events of D8-D10 from the haze days if based on PM_{10} alone, such as 5–8 March and 8–11 April (gray rectangles in Fig. 2c), because both types of events have high PM_{10}. During those haze days, $PM_{2.5}$ concentrations are almost as high as PM_{10}, thus PM_{coarse} is at low levels, excluding those days as dust episodes. Thus, PM_{coarse} is a better indicator of dust outbreaks than PM_{10}, particularly for regions with substantial anthropogenic sources of PM.

Table 1 summarizes daily PM_{coarse} and O_3 during the reported dust episodes (D1-D10) at the three cities. PM_{coarse} is around 1000 μg/m^3 during D1-D4 over Kashgar in TD, and around 150 μg/m^3 during D5-D10 over Bayannur in GD and Beijing in NC. The duration of the dust outbreaks decreases from 3 to 7 days in TD to 2–5 days in GD and 2–4 days in NC. A clear west-to-east gradient is thus evident in the duration of the dust outbreaks as well as the corresponding mass concentrations of PM_{coarse}. Table 1 also presents the difference of PM_{coarse} and O_3 during each dust episode relative to their corresponding concentrations over three reference periods: the whole season (MAM), month, and two days before each dust episode. These reference periods are chosen because they have been widely used in previous studies (Bauer et al., 2004; Bonasoni et al., 2004; Reus et al., 2005; Soler et al., 2016; Tang et al., 2004) to calculate the reference ozone level, against which ozone changes during dust events were assessed. Compared to the seasonal mean ozone at each city, average O_3 mixing ratios during the dust episodes are lower by 5.6 and 7.1 ppbv at Kashgar and Beijing, respectively, but remain the same at Bayannur. The majority (80%) of the dust outbreak days show O_3 reductions compared to the seasonal mean. However, a few dust days experienced higher O_3, e.g. by 0.6 ppbv during D6 (13–16 April) and 4.9 ppbv during D7 (29–30 April) at Bayannur. Compared to the monthly mean at each city, average O_3 mixing ratios during the dust outbreaks are lower by 5.1 and 1.4 ppbv at Kashgar and Beijing, but higher by 2.3 ppbv at Bayannur, with only 64% of the dust outbreak days showing O_3 reductions. Compared to the two-day mean before the dust breaks, the majority (80%) of the dust outbreak days also show O_3 reductions. Therefore, although the majority of the dust days show a reduction of ozone relative to three reference periods presented above (i.e., seasonal mean, monthly mean, and prior two days), the magnitude of mean ozone changes over the known dust episodes depends on the choice of the reference period. The mixed variations of ozone during the dust episodes indicate that the influence of other factors than dust (e.g. meteorology and anthropogenic emissions) is important, which is examined in the next section.

Table 1
Summary of MEE surface daily concentrations of PM_{coarse} and O_3 during reported dust episodes (D1-D10) over three representative cities: Kashgar in TD, Bayannur in GD and Beijing in NC during spring of 2015. Differences of O_3 are obtained with three reference periods: seasonal mean, monthly mean, and prior two days.

City	Date of dust outbreaks	Duration (days)	During dust outbreaks				Differences of O_3 (ΔO3) with different reference periods (ppbv)		
			PM_{coarse} (μg/m^3)		O_3 (ppbv)				
			Mean	Standard Deviation (days > 2)	Mean	Standard Deviation (days > 2)	Seasonal mean	Monthly mean	Prior two days
Kashgar in TD	D1.0310-0316	7	854.5	423.4	26.3	4.1	−6.2	−4.1	−10.9
	D2.0403-0408	6	753.5	345.8	30.9	2.0	−1.7	−1.4	−5.2
	D3.0429-0501	3	1447.4	1041.2	26.4	1.1	−6.2	−5.9	−7.0
	D4.0510-0512	3	1565.5	753.6	21.0	4.4	−11.5	−13.9	−3.0
Bayannur in GD	D5.0327-0331	5	188.3	61.5	38.0	4.4	−2.4	1.5	−8.3
	D6.0413-0416	4	130.8	37.3	41.0	0.9	0.6	1.5	2.9
	D7.0429-0430	2	106.6	N/A	45.3	N/A	4.9	5.8	14.0
Beijing in NC	D8.0319-0320	2	141.7	N/A	22.9	N/A	−12.4	−1.5	−3.5
	D9.0328-0330	3	208.5	13.2	30.3	5.3	−4.9	5.9	−8.6
	D10.0415–0418	4	134.9	29.0	29.2	7.5	−6.1	−6.7	−9.5

4. The influence of local meteorology on ozone

Besides being influenced by dust, surface ozone depends on both emissions and meteorological conditions, the latter being the primary driver of ozone day-to-day variations (Davis and Speckman, 1999; Elminir, 2005; Steiner and Finlayson-Pitts, 2010). Meteorological factors (e.g. radiation, T, RH, and winds) can influence photochemical and dispersion processes related to ozone formation (Bloomfield et al., 1996; Camalier et al., 2007; Leibensperger et al., 2008). Among so many meteorological factors, T and RH are thought to be the key ones for surface ozone. Camalier et al. (2007) suggested that ozone is generally increasing with increasing temperature and decreasing with increasing RH. Steiner and Finlayson-Pitts (2010) showed a direct linear relationship between ground level O_3 concentrations and surface air temperature. Pearce et al. (2011) estimated that the most significant meteorological variable for O_3 was temperature with increasing temperature being associated with increasing ozone, and the impacts of other variables (water vapor pressure, UV, mean sea-level pressure, radiation, boundary layer height and precipitation) were less pronounced. Zhang et al. (2016) found that ozone extreme days were most sensitive to daily maximum temperature, followed by daily minimum relative humidity, with the least sensitivity to daily minimum wind speed.

There are two significant aspects of meteorological factors controlling ozone variability in this study, as illustrated by observations at the three cities presented above (Fig. 2). First, O_3 typically has an increasing trend in springtime as a result of increasing temperature and radiation from early to late spring. For example, O_3 increases gradually from 22.9 ppbv on 1 March to 54.6 ppbv on 31 May in Beijing. Second, there are large day-to-day O_3 variations even during low dust days, presumably resulting from large day-to-day variability in meteorological conditions in spring, a transition season. For example, excluding those large dust outbreaks (D1-D10), the standard deviation of daily ozone is typically at 21% (9.9–35.1%) of the monthly mean ozone at the three cities. Therefore, the important role of meteorological factors on daily surface O_3 variations in springtime needs to be quantified before one can attribute ozone differences between dust and non-dust days to dust effects.

In order to achieve this objective, we link time series of ozone with local meteorological observations using generalized additive models (GAMs). GAMs are regression models where smoothing splines are used instead of linear coefficients for covariates (Hastie and Tibshirani, 2004). This approach has been found particularly effective at handling the complex non-linearity between air pollution and meteorology (Barmpadimos et al., 2012; Carslaw et al., 2007; Dominici et al., 2002; Pearce et al., 2011; Schlink et al., 2006; Wood et al., 2015; Zhang et al., 2017). The additive models have the general formula (1).

$$g(y_i) = \beta_0 + \sum_{j=1}^{n} s_j(x_{ij}) + \varepsilon_i \quad (1)$$

where y_i is the ith air pollution concentration, $g(y_i)$ is the "link" function, which specifies the relationship between the linear formulation on the right side of the equation and the expected response y_i, β_0 is the overall mean of the response, n is the total number of covariates (e.g. meteorological factors), $s_j(x_{ij})$ is the smooth function of ith value of covariate j, and ε_i is the ith residual with $\mathrm{var}(\varepsilon_i) = \sigma^2$, which is assumed to be normally distributed. Smooth functions are developed through a combination of model selection and automatic smoothing parameter selection using penalized regression splines, which optimize the fit with the least number of dimensions in the model (Wood et al., 2015).

In this study, the additive model for ozone can be written as:

$$\begin{aligned} g(O_3) = {} & \beta_0 + s(O_3\_prior) + s(day) + s(year) + s(dow) + s(lon, lat) \\ & + s(T) + s(RH) + s(wind\ speed) + s(msl) + s(ssr) + s(blh) \\ & + s(tp) + s(PM_{coarse}) + \varepsilon \end{aligned} \quad (2)$$

where O_3_prior is a one-day lag term (i.e. O_3 of the previous day) included to account for short-term temporal persistence, *day* is a number between 1 and 92 representing days during MAM, *year* is the year of 2015–2017, *dow* is the day of week, *lon* and *lat* are the spatial coordinates of each MEE surface monitor location over the study region (TD, GD and NC), *T* is daily temperature (unit: ˚C), *RH* is daily relative humidity (unit: %), *wind speed* is daily wind speed (unit: m/s), *msl* is mean sea-level pressure (unit: hPa), *ssr* is surface net solar radiation (unit: MJ/m^2), *blh* is boundary layer height (unit: m), *tp* is total precipitation (unit: mm), and PM_{coarse} is daily PM_{coarse} concentration, which is the indicator of dust event influence.

The GAM model (2) explains 70.2% of the variance of O_3 and provide partial response functions showing the effect of individual explanatory variables on ozone after accounting for the effects of all the other variables, i.e. accounting for any inter-correlation that may exist among the explanatory variables. A variable with p-value (p) < 0.01 is regarded as being statistically significant in explaining the ozone variability, and the variable with highest F statistics is most important. The most significant meteorological variable for O_3 is T ($F = 388.0$, $p < 0.001$). The partial response plot for T (Fig. 3a) identifies a positive non-linear relationship with increasing temperature being associated with increasing ozone. The less important variables are RH ($F = 65.0$, $p < 0.001$) and wind speed ($F = 89.9$, $p < 0.001$). Fig. S1 shows that other meteorological factors (i.e. mean sea-level pressure, surface net solar radiation, boundary layer height and total precipitation) were not significantly related to O_3 because of their strong correlations with T, RH, and wind speed. Thus, the strongest effects to O_3 by meteorology were exerted by T, followed by wind speed and RH.

The GAM model indicates that the effect of PM_{coarse} (i.e. the indicator of dust influence) on ozone is less important ($F = 23.6$, $p < 0.001$) than meteorology (T, RH, and wind speed) but still statistically significant. The partial response of O_3 to PM_{coarse} is as large as -20 ppbv during strong dust events. However, there are large uncertainties associated with such response when $PM_{coarse} > 4000\ \mu g/m^3$, the partial response ranging from -5 ppbv to -30 ppbv. As strong winds are often associated with higher levels of dust particles, high levels of PM_{coarse} are strongly correlated with high wind speeds (Fig. S2). Therefore, the effect of wind speeds on ozone is partially accounted for by dust (or PM_{coarse} in this study) when comparing ozone between dust and non-dust days, as done in many previous studies and also in the next section. Thus, the remaining significant meteorological factors are T and RH, and we control their effects on ozone differences between dust and non-dust days in the next section.

5. Differences of O_3 between dust and non-dust days

We utilize daily PM_{coarse} derived from the MEE observations to identify dust days, and then for each dust day, we look for a small subset of non-dust days that have similar meteorological conditions as the dust day as a way to minimize the compounding effects of meteorology. For each grid with available MEE observations, dust days are defined as those with daily mean PM_{coarse} exceeding the 90th percentile of the whole season's daily PM_{coarse} for that grid, and non-dust days are those below the 50th percentile. Since the dust and non-dust days are selected using grid-specific PM_{coarse} distributions, our approach thus considers the likely large across-grid differences in dust. The second step is to select a reference non-dust day for each dust day by the similarity in meteorology based on temperature (T) and relative humidity (RH), which are identified in the previous section as the most important meteorological factors affecting ozone variability during the study period/region. For a given dust day with daily mean surface

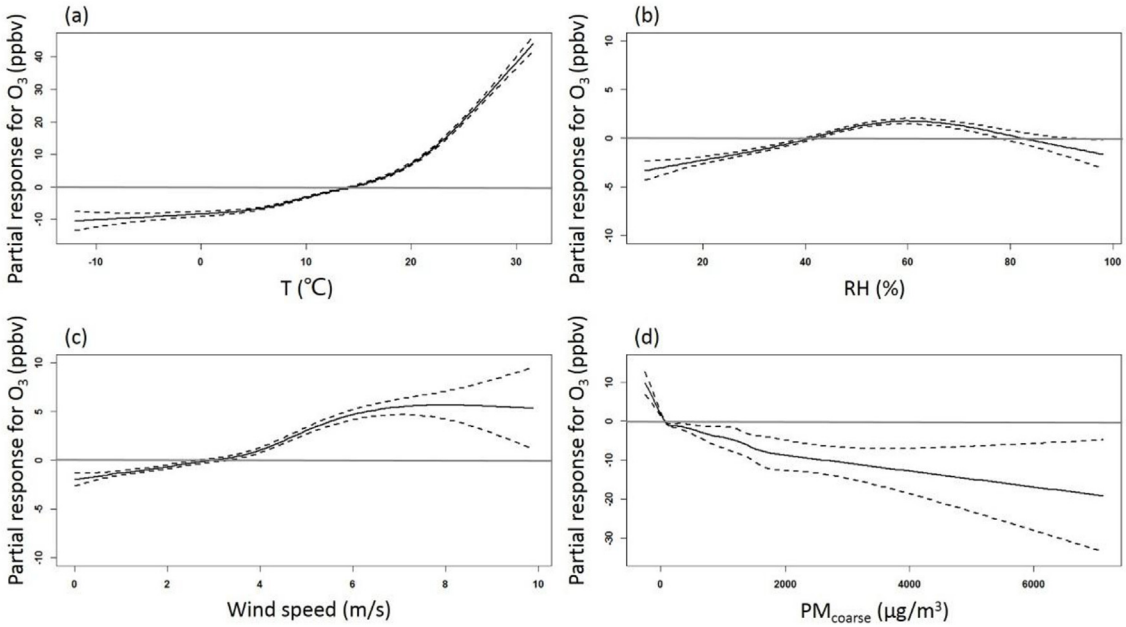

Fig. 3. Partial response plots for O_3 to T (a), RH (b), wind speed (c) and PM_{coarse} (d). The y-axis represents the marginal effects. The dashed lines are estimated 95% confidence intervals.

Table 2
Definitions of dust days and non-dust days on each grid using PM_{coarse}, temperature (T) and relative humidity (RH) during spring 2015. T_d and RH_d are the daily mean surface temperature and relative humidity of dust days, and T_{nd} and RH_{nd} are the daily mean surface temperature and relative humidity of their corresponding non-dust days. If a dust day cannot be matched with a reference non-dust day satisfying such conditions, it is disregarded from further analysis because we cannot find a reference ozone level, against which to evaluate the dust effect on ozone.

Conditions	Descriptions
Dust days	1) $PM_{coarse} \geq$ the 90th percentile of the whole season's daily concentrations 2) There exist a reference non-dust day as defined below
Non-dust days	①PM_{coarse} < the 50th percentile of the whole season's daily concentrations ②T_d - 2 °C < T_{nd} < T_d + 2 °C ③RH_d - 10% < RH_{nd} < RH_d + 10%

temperature (T_d) and relative humidity (RH_d), its reference non-dust day(s) will be those non-dust days at the same grid with surface temperature of $T_d \pm 2$°C and relative humidity of $RH_d \pm 10$ %. The range of ± 2 °C for temperature and ± 10 % for RH are chosen somewhat arbitrarily so that at least 60% of the dust days selected from the first step (i.e. using the PM_{coarse} criteria) have their corresponding non-dust days for each grid. On average, T and RH differ by less than ± 1 °C and ± 5 % respectively between dust days and their reference non-dust days for all the grids. Table 2 summarizes the definition of dust days and their reference non-dust days. If a dust day cannot be matched with a reference non-dust day satisfying such conditions, it is disregarded from further analysis because a reference ozone level cannot be established, against which to evaluate the dust effect on ozone for that day. The dust and non-dust days hereafter all refer to those satisfying the selection conditions in Table 2.

After controlling for meteorology, we assume that the ozone difference between a dust day and its corresponding non-dust day(s) can be attributed primarily to the effects of dust on ozone. For simplicity, such ozone difference is referred to as dust-associated ozone difference hereafter. Sometimes a dust day can be matched with multiple non-dust days, which all meet the conditions described above; in such cases we take the average ozone of those non-dust days to represent the non-dust ozone level. The dust-associated ozone difference is calculated for each dust day at each grid, and then aggregated temporally and spatially. The effect of dust on other species can be calculated in the same way, and the resulting difference of a given species is called the dust-associated difference of that species.

There are 34, 359, and 580 dust days with matching non-dust days over TD, GD, and NC, respectively, for which the dust-associated ozone differences are calculated. The large difference in the number of dust days in each region is mainly caused by the large difference in available site numbers: the number of grids with available observations is 5, 42, and 79 grids in TD, GD, and NC, respectively. Fig. 4 displays the relative frequency distribution of dust-associated O_3 differences for all the dust days by region. The dust-associated ozone difference is negative at 88%, 64% and 71% of the dust days for TD, GD, and NC, respectively. The corresponding magnitude of dust-associated O_3 differences, on average, is −8.8 ppbv (−22.0%), −2.2 ppbv (−4.5%), and −5.3 ppbv (−14.4%), respectively. All three regions combined, there are 70% of the dust days that show ozone reductions relative to their matching non-dust days. The predominantly negative ozone differences between the dust and non-dust days indicate that the main effect of dust on surface ozone is to decrease its concentration, possibly via the direct ozone uptake mechanism and/or precursor uptake mechanism presented above.

The calculated dust-associated ozone difference exhibits a larger variation when the PM_{coarse} difference between dust and non-dust days is relatively small (e.g. less than 200 μg/m^3), as shown in Fig. S3. Such conditions occur more often in NC where combustion-related sources play a dominating role in the pollution mix. When the PM_{coarse} difference becomes larger than 500 μg/m^3, the dust-associated ozone difference is more negative. For example, there are 74% of individual dust days showing O_3 reductions when PM_{coarse} differences are greater than 200 μg/m^3, and this proportion increases to 84.5% when PM_{coarse} differences are greater than 500 μg/m^3. This change may be related to two factors: (1) the accuracy of using PM_{coarse} as an indicator of dust would increase when this difference is large, especially outside of dust source regions (e.g. NC); and (2) there would be a general tendency of increasing ozone reduction with increasing dust levels. The second factor

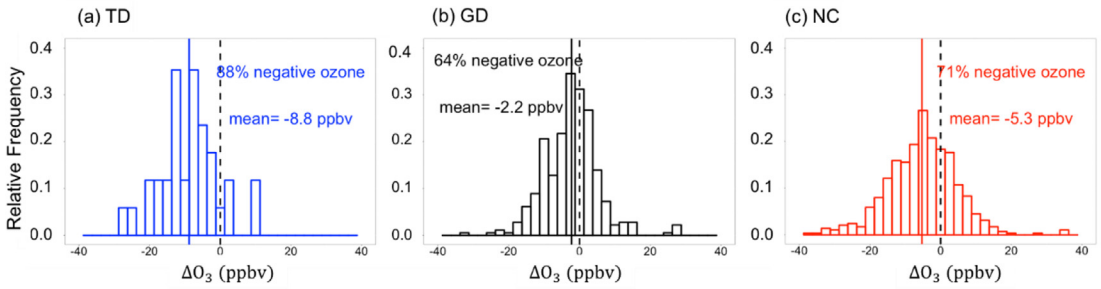

Fig. 4. Relative frequency distribution of dust-associated O_3 differences for all dust days over TD (a), GD (b) and NC (c). Blue, black and red bins are results for TD, GD and NC. Regional mean O_3 differences and percentages of dust days showing negative O_3 over these three regions are also shown in the figure. Solid lines are regional mean dust-associated O_3 differences of the three regions, and dashed black lines are for zero. The width of bins is five ppbv. (For interpretation of the references to colour in this figure legend, the reader is referred to the Web version of this article.)

has been seen in laboratory studies. Measured O_3 uptake coefficients by mineral dust were found to increase linearly with increasing sample mass at low levels and reach to an upper limit where a mass-independent plateau region was observed (Michel et al., 2002; Nicolas et al., 2009).

Fig. 5 shows the spatial distributions of seasonal-mean dust-associated ozone differences (a) and PM_{coarse} differences (b) at each grid during spring 2015. The regional-mean statistics for the dust-associated differences in ozone and other pollutants are summarized in Table 3. For seasonal mean, the dust-associated ozone difference is negative at 100%, 83% and 91% of the grids for TD, GD, and NC, respectively (Table 3). O_3 mixing ratios, on average, are lower by 10.1 ppbv (24.6%), 2.4 ppbv (4.8%), and 5.4 ppbv (14.3%) over the three regions during dust days compared to their non-dust counterparts with similar meteorology. Seasonal mean PM_{coarse} differences between dust and non-dust days (Fig. 5b) exhibit a clear west-to-east gradient from 942.3 μg/m^3 in TD to 191.1 μg/m^3 in GD and 113.9 μg/m^3 in NC, indicative of the west-to-east transport pathway of dust.

To investigate the influence of local anthropogenic emissions on O_3 during dust days, we calculated the differences of NO_2, SO_2 and CO using the same method as calculating the ozone difference between dust and non-dust days, and the results are shown in Fig. 6. Compared to non-dust days, average NO_2, SO_2, and CO mixing ratios during dust days are almost the same over TD and GD (Table 3), but higher by 6.3 ppbv, 4.5 ppbv and 0.3 ppmv, respectively, over NC (Fig. 6). Over TD and GD, the little difference of these primary pollutants between dust and non-dust days may be due to the fact that their concentrations are low over these regions and could be interpreted to support the mechanism of dust direct uptake of O_3. Over NC, the higher level of those species during the dust days is indicative of more polluted conditions, presumably due to reduced dispersion conditions and/or higher anthropogenic emissions. These conditions make it difficult to estimate the effect of acid uptake by dust that may occur. For example, a modeling study (Wang et al., 2017) estimated that heterogeneous reactions

Table 3
Regional-mean statistics for the dust-associated differences of ozone and other air pollutants over TD, GD and NC during spring 2015.

Regions	TD	GD	NC
grids of O_3 reductions	5	35	72
grids of O_3 increase	0	7	7
Percent of grids showing O_3 reductions (%)	100	83.3	91.1
Mean value of O_3 differences (ppbv)	−10.1	−2.4	−5.4
Mean value of O_3 differences (%)	−24.5	−4.8	−14.3
Mean value of PM_{coarse} differences (μg/m^3)	942.3	191.1	113.9
Mean value of NO_2 differences (ppbv)	0.1	−0.4	6.3
Mean value of SO_2 differences (ppbv)	0	−0.3	4.5
Mean value of CO differences (ppmv)	0.1	0	0.3

on dust lead to production of nitrate and sulfate on both coarse (100% for both species) and fine (17% for nitrate and 11% for sulfate) modes dust particles during dust events over northern China. To tease out such effects from ambient measures would require speciation measurements of $PM_{2.5}$ and PM_{10} which we do not have. Since higher air pollutants conditions would typically be associated higher ozone levels in the absence of dust influences, especially considering NO_2 is a precursor for ozone, the fact that surface ozone levels were significantly lower during the dust days over NC also lends support to the mechanism of dust direct uptake of O_3.

To summarize, through quantifying O_3 changes between dust and non-dust days by controlling meteorological factors, we found that the majority of individual dust days and individual grids over the three study regions had lower O_3 levels during dust days. When the PM_{coarse} difference during individual dust days becomes larger, indicating larger dust outbreaks, O_3 is more likely to be reduced and the magnitude of the reduction also becomes larger. NO_2, SO_2 and CO were higher during dust days outside the dust source regions (e.g. NC), possibly because of the compounding effects of large anthropogenic emissions over this region. In spite of similar or higher levels of anthropogenic emissions,

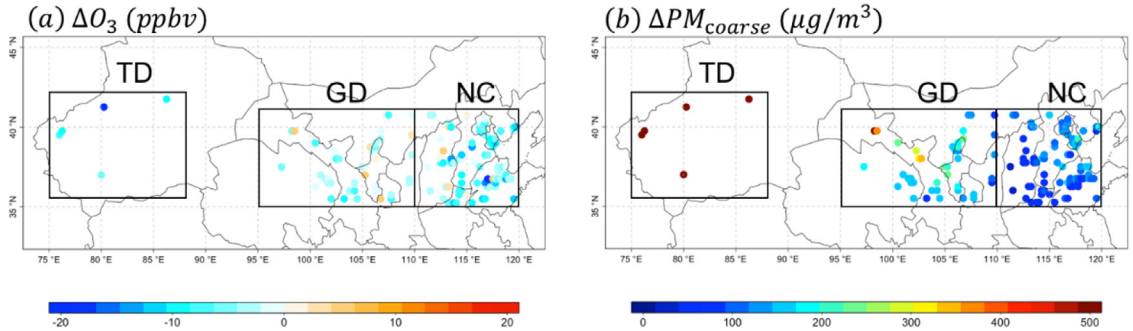

Fig. 5. Spatial distribution of seasonal-mean dust-associated O_3 (a) and PM_{coarse} (b) differences at each grid over TD, GD and NC during spring of 2015. Rectangles outline TD, GD and NC.

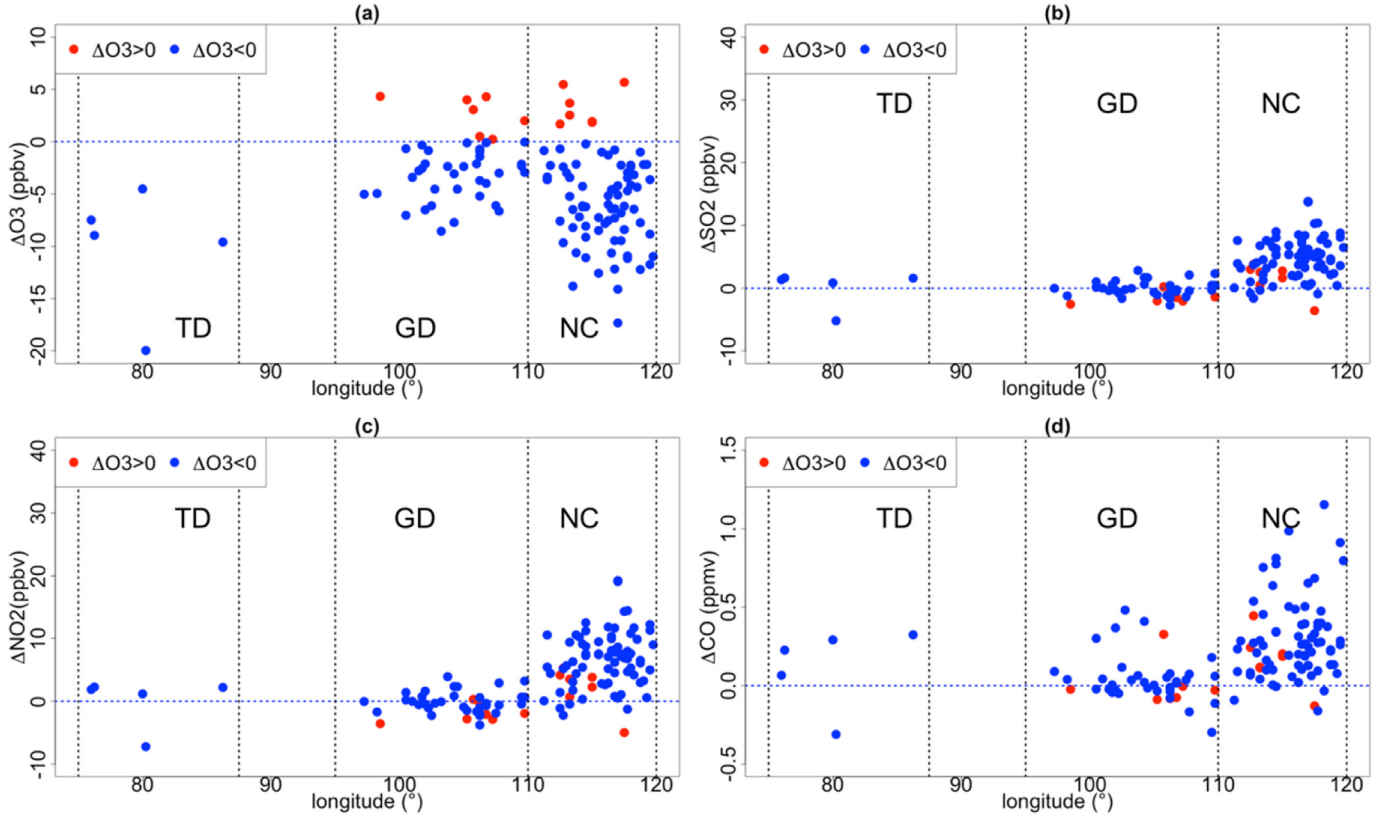

Fig. 6. Grid-mean dust-associated differences of surface daily O_3 (a), SO_2 (b), NO_2 (c), and CO (d) concentrations along longitude over TD, GD, and NC during spring 2015. Red and blue spots outline grids, in which the dust-associated O_3 differences are more than and less than zero, respectively. (For interpretation of the references to colour in this figure legend, the reader is referred to the Web version of this article.)

surface ozone concentrations are still lower during dust days over TD, GD and NC, supporting the mechanism of dust direct uptake of O_3 instead of via changing ozone precursors. The analyses of the spring 2016 and 2017 data give similar results to those of 2015 and are shown in the supplementary material (Table S2-S3 and Fig. S4-S5).

6. Discussions

The previous section presents the dust-ozone relationship in springtime of 2015 for Asian dust. PM_{coarse} is used as an indicator of dust influences because we do not have observations of mineral dust with good temporal and spatial coverage in China. Temporally, surface O_3 mixing ratios are found to be on average lower by 8.8 ppbv (22%), 2.2 ppbv (4.5%) and 5.3 ppbv (14.4%) over TD, GD and NC during the dust days compared to their non-dust counterparts with similar meteorology defined by T and RH. Spatially, the seasonal-mean surface O_3 reductions during the dust days are −10.1 ppbv (−24.6%), −2.4 ppbv (−4.8%) and −5.4 ppbv (−14.3%) for the three regions. In this section, we discuss the comparison of our results to previous field studies, mechanisms, and limitations.

6.1. Comparison to previous field studies

Table 4 summarizes published field studies of the dust-ozone relationship by dust type, time period, location, and observed dust level and ozone change. The majority of these studies (Andrey et al., 2014; Bonasoni et al., 2004; Jenkins et al., 2012; Reus et al., 2005; Soler et al., 2016) reported measurements of Saharan dust episodes at one or a few European sites over time periods ranging from a few days to seven months. Tang et al. (2004) and Fairlie et al. (2010) presented month-long aircraft measurements of Asian dust over the Yellow Sea and the northeast Pacific respectively. The present study examines the dust-ozone relationship of Asian dust using seasonal-long daily air quality observations at more than 100 surface grids in China along the dust transport route from the source region TD in the west and GD in the central, to the receptor region NC in the east. We focus on the ozone response within and close to the dust source regions and have a better spatial and temporal coverage of observations than previous field studies.

To compare ozone changes between different dust episodes, we first compare dust levels between the different field studies. In the present study, seasonal mean PM_{coarse} differences between dust and non-dust days (Fig. 5b) are 942.3 μg/m^3 in TD (major source region), 191.1 μg/m^3 in GD (secondary source region), and 113.9 μg/m^3 in NC (non-source region). PM_{10} concentrations during Saharan dust episodes in the Po valley were around 50 μg/m^3 with peaks reaching about 150 μg/m^3 (Bonasoni et al., 2004). This is similar to PM_{10} observed at the Bayannur site in GD (Fig. 2b). Reus et al. (2005) showed a similar record of PM_{10} mass concentrations, which increased from 13 μg/m^3 to 190 μg/m^3 during dust events on a mountain ridge on the island of Tenerife (28°18′N, 16°29′E). Tang et al. (2004) detected a higher level of hourly coarse dust concentrations reaching 500–2500 μg/m^3 at 2–6 km above sea level (ASL) over the Yellow Sea, which is qualitatively similar to the PM_{coarse} differences over the TD at the surface.

The regional-mean dust-associated O_3 reductions in the present study are −10.1 ppbv (−24.6%), −2.4 ppbv (−4.8%), and −5.4 ppbv (−14.3%) over TD, GD and NC respectively, which are qualitatively similar to the ozone effects attributed to Saharan dust in previous field studies. Bonasoni et al. (2004) measured that ozone mixing ratios during Saharan dust events were 4%–21% lower than the monthly mean background values in Mt. Cimone, and 2.7% to 12.8% lower than the seasonal mean in the Po valley. Reus et al. (2005) found 17–22 ppbv of O_3 reductions during dust events on a mountain ridge on the island of Tenerife. Soler et al. (2016) recorded an average ozone reduction of

Table 4
Published field studies of the dust-ozone relationship by dust type, time period, location, observed dust level and ozone change. Altitudes of sites are above sea level (ASL).

Saharan dust	Time period	Location	Observed dust level		Ozone change	
Bonasoni et al., 2004	June–December 2000	Mt. Cimone (44°11′N, 10°42′E; 2165 m ASL)	Mean volume concentration for coarse dust	+5.55 $\mu m^3/cm^3$	Compared to monthly mean	−4%～ −21% (−3～-5 ppb)
		Po valley (10 m–56 m ASL)	PM10 compared to seasonal mean	+19.2% ～ +36.7%	Compared to seasonal mean	−2.70%～ −12.80%
Reus et al., 2005	28–31 July 2002	Tenerife (28°18′N, 16°29′E: 2360 m ASL)	PM10	daytime +173 $\mu g/m^3$	Ozone	daytime −17 ppbv
				nighttime +187 $\mu g/m^3$		nighttime −22 ppbv
Andrey et al., 2014	June–September 1997–2011	Canary Islands (28.1°N, 15.4°W; 0–8 km ASL)	Between non-SAL and SAL	+50～+500 $\mu m^3/cm^3$	Between non-SAL and SAL	−35–15%
Jenkins et al., 2012	25 June- 17 July 2010	Cape Verde (16.84°N, 24.87°E; 200–1000 hPa)			Between non-SAL and SAL	−20～-30 ppbv
Soler et al., 2016	May–September 2012	Aitana (38°16′N; 0°41′W; 1558 m ASL)	Coarse dust	+0.10～+1.14 cm^{-3}		-5.5% (max −15%)
Asian dust						
Tang et al., 2004	0000-0800 GMT 04/11/2001	The Yellow Sea (35–38°N,125–131°E; 0–6500 m ASL)	Coarse dust	+500～+2500 $\mu g/m^3$		−20 ppbv
Fairlie et al., 2010	21 April-11 May 2006	The northeast Pacific (1–11 km ASL)	AOD 0.1–0.4			no detectable ozone change
this study	March–May 2015	TD	The "dust associated" PM_{coarse} differences	+942.3 $\mu g/m^3$	The "dust associated" Ozone differences	−10.1 ppbv (−24.6%)
		GD		+191.1 $\mu g/m^3$		−2.4 ppbv (−4.8%)
		NC		+113.9 $\mu g/m^3$		−5.4 ppbv (−14.3%)

5.5% during Saharan events at a mountain station located near the eastern coast of the Iberian Peninsula from May to September 2012.

There are however contradictory conclusions from previous field studies on the effects of Asian dust on ozone. Tang et al. (2004) showed a reduction of 20 ppbv in hourly O_3 mixing ratio during one Asian dust outflow episode sampled by an aircraft campaign over the Yellow Sea in spring 2001. Fairlie et al. (2010) did not detect O_3 depletion in Asian dust plumes encountered during another aircraft campaign in spring 2006 over the northeast Pacific, which seems to be an outlier with respect to observational studies of ozone in dust plumes. The aircraft data in Fairlie et al. (2010) were snap-shots of atmospheric composition a few thousands of kilometers downwind of Asia. The reason why such data did not show ozone reduction associated with Asian dust can be attributed to several reasons. First, Asian dust concentrations are lower over the northeast Pacific. The present study examined the ozone-dust relationship within and close to the dust source regions in China, providing more direct observational evidence of ozone reduction by Asian dust. In addition, we found the magnitude of the dust-associated O_3 reduction has a general tendency of decreasing with decreasing PM_{coarse} mass concentration, the proxy of dust levels. When Asian dust aerosols are transported to the northeast Pacific, the concentration is expected to decrease, leading to a tendency of less ozone reductions by dust. The second reason is the compounding effects of meteorology on ozone. We found meteorology plays a large role in controlling day-to-day O_3 variability. Such effect needs to be removed or at least controlled in order to isolate the dust effect on ozone. To control the meteorology effect, we used a season's worth of data to define a reference non-dust day with similar meteorology as each dust day. However, due to the short period of the aircraft campaign analyzed by Fairlie et al. (2010), their work did not control for the effect of meteorology in causing the O_3 variations in the dust episode. Third, the ozone uptake effect may be muted by the mixture of dust with anthropogenic air pollutants during trans-Pacific transport. By the time they reach the northeast Pacific, the properties of Asian dust would have been significantly influenced by anthropogenic pollutants from polluted eastern China. Some studies suggested that Asian dust particles can be converted into aqueous droplets forming $Ca(NO_3)_2$ and $CaCl_2$ in the vicinity of strong anthropogenic emission sources (Tang et al., 2016; Tobo et al., 2010). O_3 uptake coefficients by dust were found to be different on the different mineralogy of dust particles in laboratory studies (Crowley et al., 2010; Usher et al., 2002). In addition, measured O_3 uptake coefficients by mineral dust were found to decrease with increasing relative humidity (Crowley et al., 2010).

6.2. Mechanisms

The majority of previous modeling studies suggested that heterogeneous reactions play the dominant role in the effect of dust on O_3. Light scattering by dust particles leads to a decrease of direct radiation but an increase of diffusive radiation in the lower atmosphere, and the combined effect was found to be small for photolysis rate calculation. Liao et al. (2003) suggested that the inclusion of aerosols in photolysis resulted in less than 0.2 ppbv change of monthly mean O3. Bian and Zender (2003) showed a 0.2% increase of annual-mean O_3 globally due to the impact of mineral dust on photolysis rates. Tang et al. (2004) estimated that the dust radiative influence was responsible for a 1 ppbv ozone decrease during the dust episode they observed above the Yellow Sea, compared to that of 20–30 ppbv attributed to heterogeneous reactions on dust. According to these modeling studies, we presume that the predominant feature of ozone reduction during dust days over TD, GD, and NC is caused primarily by heterogeneous reactions on dust.

The uptake of NO_2 by heterogeneous reactions on dust forms more soluble nitrates, which acts to reduce ozone (Fairlie et al., 2010; Wang et al., 2012, 2017). However, NO_2 is found to be higher over NC during dust days, indicating other factors may dominate the dust effect. As a precursor for ozone, higher levels of NO_2 would increase ozone levels

and reduce the effect of dust uptake of ozone during dust days. The fact that surface ozone levels are still significantly lower during the dust days over NC suggests that the mechanism is via dust direct uptake of O_3, rather than the indirect effect of dust uptake of ozone precursors (i.e. NO_2). Over TD and GD, little difference of these primary pollutants between dust and non-dust days may be due to the fact that their concentrations are low over these regions and could also be interpreted to support the mechanism of dust direct uptake of O_3. Therefore, in spite of higher or similar levels of primary pollutants, surface ozone concentrations are still lower during dust days over TD, GD and NC, supporting the mechanism of dust direct uptake of O_3 instead of via changing ozone precursors.

6.3. Limitations

The main limitation of the present study is the use of PM_{coarse} as an indicator of dust influences due to the lack of direct measurement of dust levels. In particular, PM_{coarse} does not include fine-mode dust. Since fine-mode dust is expected to co-occur with coarse-mode dust during major dust episodes, PM_{coarse} is used as an indicator of the timing of dust events, but it is not a good measure of dust concentrations. That is why we do not find a good negative correlation between PM_{coarse} and the dust-associated ozone difference.

The second limitation is the use of NO_2, SO_2 and CO as indicators of precursor influences due to the lack of direct measurement of nitrous oxide (NO_x) and volatile organic compounds (VOCs). Ground-level O_3 is classified as a secondary air pollutant because it is produced in the atmosphere when precursors such as NO_x and VOCs react under sunlight. Precursors can be produced from different sorts of emissions. NO_2 and SO_2 can be used as an indicator for NOx and VOCs from anthropogenic emissions (Zhang et al., 2009). Although CO is often not correlated with biogenic VOCs, it can be used as an indicator for VOCs from biomass burning (Simpson et al., 2011) and residential solid fuel. For biogenic VOCs from natural sources, we assume that they are similar under the same levels of T and RH (Guenther et al., 2012). Therefore, under similar meteorology conditions, NO_2, SO_2 and CO in combination can be used as indicators for precursors. With regard to the year-to-year differences in the dataset analyzed here, Table S4 shows an increasing trend for regional-mean NO_2, SO_2 and O_3 over TD, GD and NC during spring 2015–2017, with a decreasing trend for regional-mean CO. Thus, interannual variation is a significant variable for O_3 ($F = 947.0$, $p < 0.001$) in the GAM model (2). Therefore, we analyzed the dust-associated difference analysis year by year instead of combing three years together.

The third limitation is the spatial coverage. First, the MEE surface network has limited spatial coverage, particularly over the dust source regions. Furthermore, we only analyzed surface O_3, whereas the dust influence on ozone has been found to be more significant in the free troposphere (Andrey et al., 2014; Jenkins et al., 2012). The Saharan dust layer observed in the free troposphere is typically a distinct one-layer structure below 5 km ASL. By comparison, a vertically two-layered dust distribution was observed during Asian dust outbreaks (Eguchi et al., 2009; Nan and Wang, 2018; Sun et al., 2001). The lower dust layer from the Gobi Desert is transported at an altitude less than 4 km ASL and likely mixed with Asian anthropogenic air pollutants. The upper dust layer mainly originates from the Taklimakan Desert and is transported in higher altitude around 5–12 km ASL above the major clouds layer and almost unaffected by Asian air pollutants and wet removal. Therefore, future work should be conducted to understand the effects of those dust layers on vertical ozone distribution.

7. Conclusions

In this study we have investigated the impacts of Asian dust on surface O_3 over northern China on a daily scale using observations from recently established network of surface air quality monitors and meteorology reanalysis data during spring (March, April, May; MAM) 2015–2017 with a focus on 2015. Here we use the coarse particulate matter mass concentrations (PM_{coarse}) as an indicator of dust influences because we do not have observations of mineral dust with good temporal and spatial coverage in China.

We select dust days and their reference non-dust days based on the distribution of daily PM_{coarse}, temperature (T), and relative humidity (RH). The T and RH criteria are used to minimize the effect of different meteorological conditions between a dust day and its reference non-dust day. Temporally, surface O_3 mixing ratios are found to be on average lower by 8.8 ppbv (22%), 2.2 ppbv (4.5%) and 5.3 ppbv (14.4%) over TD, GD and NC during the dust days compared to their non-dust counterparts with similar meteorology defined by T and RH. Spatially, the seasonal-mean surface O_3 reductions during the dust days are −10.1 ppbv (−24.6%), −2.4 ppbv (−4.8%) and −5.4 ppbv (−14.3%) for the three regions. The majority of dust days thus shows lower O_3 compared to non-dust days both temporally and spatially. When the PM_{coarse} difference becomes larger during individual dust days, indicating larger dust outbreaks, O_3 is more likely to be reduced and the magnitude of the reduction also becomes larger. NO_2, SO_2 and CO appear to be higher during dust days outside dust source regions (e.g. NC), possibly because of the compounding effects of large anthropogenic emissions over this region. In spite of higher or similar levels of primary pollutants, surface ozone concentrations are still lower during dust days over TD, GD and NC, supporting the mechanism of dust direct uptake of O_3 instead of via changing ozone precursors.

The dust-associated O_3 differences over TD, GD and NC are qualitatively similar to the ozone effects attributed to Saharan dust in previous field studies. According to previous modeling studies, we presume that the predominant feature of ozone reduction during dust days over TD, GD, and NC is caused primarily by heterogeneous reactions on dust. The fact that surface ozone levels are still significantly lower during the dust days over NC suggests that the mechanism is via dust direct uptake of O_3, rather than the indirect effect of dust uptake of ozone precursors (i.e. NO_2).

The limitations of the present study are the lacks of direct measurement of dust levels, ozone precursors and the spatial coverage of observations. The impact of weather conditions on surface ozone variability in China warrants a separate analysis. The dust-ozone relationship may require verification with longer-term observations when more data become available in the future. The relationship between dust and surface ozone variations identified here provides a useful metric that may be used to forecast ozone concentrations and evaluate model performance in simulating meteorological drivers of ozone variability in northern China.

Acknowledgment

This research was supported by the National Key Basic Research Program of China (2013CB956603 and 2014CB441302) and the CAS Strategic Priority Research Program (Grant No. XDA05100403).

Appendix A. Supplementary data

Supplementary data related to this article can be found at http://dx.doi.org/10.1016/j.atmosenv.2018.05.032.

References

Andrey, J., Cuevas, E., Parrondo, M.C., Alonso-Pérez, S., Redondas, A., Gil-Ojeda, M., 2014. Quantification of ozone reductions within the Saharan air layer through a 13-year climatologic analysis of ozone profiles. Atmos. Environ. 84, 28–34.

Barmpadimos, I., Keller, J., Oderbolz, D., Hueglin, C., T, A.S.H.P., 2012. One decade of parallel fine (PM2.5) and coarse (PM10–PM2.5) particulate matter measurements in Europe: trends and variability. Atmos. Chem. Phys. 12, 3189–3203.

Bauer, S.E., Balkanski, Y., Schulz, M., Hauglustaine, D.A., Dentener, F., 2004. Global modeling of heterogeneous chemistry on mineral aerosol surfaces: influence on tropospheric ozone chemistry and comparison to observations. J. Geophys. Res.: Atmos.

109.
Bian, H., Zender, C.S., 2003. Mineral dust and global tropospheric chemistry: relative roles of photolysis and heterogeneous uptake. J. Geophys. Res.: Atmos. 108.
Bloomfield, P., Royle, J.A., Steinberg, L.J., Yang, Q., 1996. Accounting for meteorological effects in measuring urban ozone levels and trends. Atmos. Environ. 30, 3067–3077.
Bonasoni, P., Cristofanelli, P., Calzolari, F., Bonafè, U., 2004. Aerosol-ozone correlations during dust transport episodes. Atmos. Chem. Phys. 4, 1201–1215.
Camalier, L., Cox, W., Dolwick, P., 2007. The effects of meteorology on ozone in urban areas and their use in assessing ozone trends. Atmos. Environ. 41, 7127–7137.
Carslaw, D.C., Beevers, S.D., Tate, J.E., 2007. Modelling and assessing trends in traffic-related emissions using a generalised additive modelling approach. Atmos. Environ. 41, 5289–5299.
Crowley, J.N., Ammann, M., Cox, R.A., Hynes, R.G., 2010. Evaluated kinetic and photochemical data for atmospheric chemistry: volume V–heterogeneous reactions on solid substrates. Atmos. Chem. Phys. 10, 9059–9223.
Davis, J.M., Speckman, P., 1999. A model for predicting maximum and 8h average ozone in Houston. Atmos. Environ. 33, 2487–2500.
Dominici, F., Mcdermott, A., Zeger, S.L., Samet, J.M., 2002. On the use of generalized additive models in time-series studies of air pollution and health. Am. J. Epidemiol. 156, 193–203.
Donkelaar, A.V., Martin, R.V., Brauer, M., Kahn, R., Levy, R., Verduzco, C., Villeneuve, P.J., 2010. Global estimates of ambient fine particulate matter concentrations from satellite-based aerosol optical depth: development and application. Environ. Health Perspect. 118, 847.
Eguchi, K., Uno, I., Yumimoto, K., Takemura, T., 2009. Trans-Pacific dust transport: integrated analysis of NASA/CALIPSO and a global aerosol transport model. Atmos. Chem. Phys. 9, 3137–3145.
Elminir, H.K., 2005. Dependence of urban air pollutants on meteorology. Sci. Total Environ. 350, 225–237.
Fairlie, T.D., Jacob, D.J., Dibb, J.E., Alexander, B., 2010. Impact of mineral dust on nitrate, sulfate, and ozone in transpacific Asian pollution plumes. Atmos. Chem. Phys. 10, 3999–4012.
Feng, X.Y., Wang, S.G., Yang, D.B., Shang, K.Z., 2011. Influence of dust EventsonPM10 pollution in key environmental protection cities of northern China during recent years. J. Desert Res. 31, 735–740.
Ginoux, P., Chin, M., Tegen, I., Prospero, J.M., Holben, B., Dubovik, O., Lin, S.J., 2001. Sources and distributions of dust aerosols simulated with the GOCART model. J. Geophys. Res.: Atmos. 106, 20255–20273.
Goodman, A.L., Li, P., And, C.R.U., Grassian, V.H., 2001. Heterogeneous uptake of sulfur dioxide on aluminum and magnesium oxide particles. J. Phys. Chem. 105, 6109–6120.
Guenther, A.B., Jiang, X., Heald, C.L., Sakulyanontvittaya, T., Duhl, T., Emmons, L.K., Wang, X., 2012. The Model of Emissions of Gases and Aerosols from Nature version 2.1 (MEGAN2.1): an extended and updated framework for modeling biogenic emissions. Geosci. Model Dev. Discuss. (GMDD) 5, 1–58.
Guo, S., Hu, M., Zamora, M.L., Peng, J., Shang, D., Zheng, J., Du, Z., Wu, Z., Shao, M., Zeng, L., 2014. Elucidating severe urban haze formation in China. Proc. Natl. Acad. Sci. 111, 17373–17378.
Hanisch, F., Crowley, J.N., 2003. Ozone decomposition on Saharan dust: an experimental investigation. Atmos. Chem. Phys. 3, 119–130.
Hastie, T., Tibshirani, R., 2004. Generalized additive models. Stat. Sci. 1, 297–310.
Huang, J., Wang, T., Wang, W., Li, Z., Yan, H., 2015. Climate effects of dust aerosols over East Asian arid and semiarid regions. J. Geophys. Res.: Atmos. 119.
Jenkins, G.S., Robjhon, M.L., Smith, J.W., Clark, J., Mendes, L., 2012. The influence of the SAL and lightning on tropospheric ozone variability over the Northern Tropical Atlantic: results from Cape Verde during 2010. Geophys. Res. Lett. 39.
Johnson, E.R., Sciegienka, J., Carloscuellar, S., Grassian, V.H., 2005. Heterogeneous uptake of gaseous nitric acid on dolomite (CaMg (CO3) 2) and calcite (CaCO3) particles: a Knudsen cell study using multiple, single, and fractional particle layers. J. Phys. Chem. 109, 6901–6911.
Kok, J.F., 2011. A scaling theory for the size distribution of emitted dust aerosols suggests climate models underestimate the size of the global dust cycle. Proc. Natl. Acad. Sci. 108, 1016–1021.
Leibensperger, E.M., Mickley, L.J., Jacob, D.J., 2008. Sensitivity of US air quality to mid-latitude cyclone frequency and implications of 1980–2006 climate change. Atmos. Chem. Phys. 8, 7075–7086.
Liao, H., Adams, P.J., Chung, S.H., Seinfeld, J.H., Mickley, L.J., Jacob, D.J., 2003. Interactions between tropospheric chemistry and aerosols in a unified general circulation model. J. Geophys. Res.: Atmos. 108.
Lv, Y., Li, D., Li, Z., Chen, X., Xu, H., Liu, Z., Qie, L., Zhang, Y., Li, K., Ma, Y., 2015. Observation of a dust storm during 2015 spring over beijing, China. In: AGU Fall Meeting Abstracts.
Michel, A.E., Usher, C.R., Grassian, V.H., 2002. Heterogeneous and catalytic uptake of ozone on mineral oxides and dusts: a Knudsen cell investigation. Geophys. Res. Lett. 29.
Nan, Y., Wang, Y., 2018. De-coupling interannual variations of vertical dust extinction over the Taklimakan Desert during 2007–2016 using CALIOP. Sci. Total Environ. 633, 608–617.
Nicolas, M., Ndour, M., Ka, O., D'Anna, B., George, C., 2009. Photochemistry of atmospheric dust: ozone decomposition on illuminated titanium dioxide. Environ. Sci. Technol. 43, 7437–7442.
Pearce, J.L., Beringer, J., Nicholls, N., Hyndman, R.J., Tapper, N.J., 2011. Quantifying the influence of local meteorology on air quality using generalized additive models. Atmos. Environ. 45, 1328–1336.
Pozzoli, L., Bey, I., Rast, S., Schultz, M.G., Stier, P., Feichter, J., 2008. Trace gas and aerosol interactions in the fully coupled model of aerosol-chemistry-climate ECHAM5-HAMMOZ: 1. Model description and insights from the spring 2001 TRACE-P experiment. J. Geophys. Res.: Atmos. 113.
Reus, M.D., Dentener, F., Thomas, A., Borrmann, S., Ström, J., Lelieveld, J., 2000. Airborne observations of dust aerosol over the North Atlantic Ocean during ACE 2: indications for heterogeneous ozone destruction. J. Geophys. Res.: Atmos. 105, 15263–15275.
Reus, M.D., Fischer, H., Sander, R., Gros, V., 2005. Observations and model calculations of trace gas scavenging in a dense Saharan dust plume during MINATROC. Atmos. Chem. Phys. 5, 1787–1803.
Rosenfeld, D., Rudich, Y., Lahav, R., 2001. Desert dust suppressing precipitation: a possible desertification feedback loop. Proc. Natl. Acad. Sci. 98, 5975–5980.
Schlink, U., Herbarth, O., Richter, M., Dorling, S., Nunnari, G., Cawley, G., Pelikan, E., 2006. Statistical models to assess the health effects and to forecast ground-level ozone. Environ. Model. Software 21, 547–558.
Shao, Y., Wyrwoll, K.H., Chappell, A., Huang, J., Lin, Z., Mctainsh, G.H., Mikami, M., Tanaka, T.Y., Wang, X., Yoon, S., 2011. Dust cycle: an emerging core theme in Earth system science. Aeolian Res. 2, 181–204.
Simpson, I.J., Akagi, S.K., Barletta, B., Blake, N.J., Choi, Y., Diskin, G.S., Fried, A., Fuelberg, H.E., Meinardi, S., Rowland, F.S., 2011. Boreal forest fire emissions in fresh Canadian smoke plumes: C1-C10 volatile organic compounds (VOCs), CO2, CO, NO2, NO, HCN and CH3CN. Atmos. Chem. Phys. 11, 6445–6463.
Soler, R., Nicolás, J.F., Caballero, S., Yubero, E., Crespo, J., 2016. Depletion of tropospheric ozone associated with mineral dust outbreaks. Environ. Sci. Pollut. Control Ser. 23, 19376–19386.
Steiner, A.L., Finlayson-Pitts, B.J., 2010. Observed suppression of ozone formation at extremely high temperatures due to chemical and biophysical feedbacks. Proc. Natl. Acad. Sci. 107, 19685–19690.
Sun, J., Zhang, M., Liu, T., 2001. Spatial and temporal characteristics of dust storms in China and its surrounding regions, 1960–1999: relations to source area and climate. J. Geophys. Res.: Atmos. 106, 10325–10333.
Tang, M., Cziczo, D.J., Grassian, V.H., 2016. Interactions of water with mineral dust aerosol: water adsorption, hygroscopicity, cloud condensation, and ice nucleation. Chem. Rev. 116, 4205–4259.
Tang, Y., Carmichael, G.R., Kurata, G., Uno, I., Weber, R.J., Song, C.H., Guttikunda, S.K., Woo, J.H., Streets, D.G., Wei, C., 2004. Impacts of dust on regional tropospheric chemistry during the ACE-Asia experiment: a model study with observations. J. Geophys. Res.: Atmos. 109.
Tegen, I., Schepanski, K., 2009. The global distribution of mineral dust. In: IOP Conference Series: Earth and Environmental Science. IOP Publishing, pp. 012001.
Tobo, Y., Zhang, D., Matsuki, A., Iwasaka, Y., 2010. Asian dust particles converted into aqueous droplets under remote marine atmospheric conditions. Proc. Natl. Acad. Sci. 107, 17905–17910.
Underwood, G.M., Song, C.H., Phadnis, M., Carmichael, G.R., Grassian, V.H., 2001. Heterogeneous reactions of NO2 and HNO3 on oxides and mineral dust: a combined laboratory and modeling study. J. Geophys. Res.: Atmos. 106, 18055–18066.
Uno, I., Eguchi, K., Yumimoto, K., Takemura, T., Shimizu, A., Uematsu, M., Liu, Z., Wang, Z., Hara, Y., Sugimoto, N., 2009. Asian dust transported one full circuit around the globe. Nat. Geosci. 2, 557–560.
Usher, C.R., Al-Hosney, H., Carlos-Cuellar, S., Grassian, V.H., 2002. A laboratory study of the heterogeneous uptake and oxidation of sulfur dioxide on mineral dust particles. J. Geophys. Res.: Atmos. 107.
Usher, C.R., Michel, A.E., Grassian, V.H., 2003. Reactions on mineral dust. Chem. Rev. 103, 4883–4940.
Wang, G., Zhang, R., Gomez, M.E., Yang, L., Levy, Z.M., Hu, M., Lin, Y., Peng, J., Guo, S., Meng, J., 2016. Persistent sulfate formation from London Fog to Chinese haze. Proc. Natl. Acad. Sci. 113, 13630–13635.
Wang, K., Zhang, Y., Nenes, A., Fountoukis, C., 2012. Implementation of dust emission and chemistry into the Community Multiscale Air Quality modeling system and initial application to an Asian dust storm episode. Atmos. Chem. Phys. 12, 10209–10237.
Wang, Y., Zhang, Q., Jiang, J., Zhou, W., Wang, B., He, K., Duan, F., Zhang, Q., Philip, S., Xie, Y., 2015. Enhanced sulfate formation during China's severe winter haze episode in January 2013 missing from current models. J. Geophys. Res.: Atmos. 119.
Wang, Z., Pan, X., Uno, I., Li, J., Wang, Z., Chen, X., Fu, P., Yang, T., Kobayashi, H., Shimizu, A., 2017. Significant impacts of heterogeneous reactions on the chemical composition and mixing state of dust particles: a case study during dust events over northern China. Atmos. Environ. 159, 83–91.
Wood, S.N., Pya, N., Sã¤Fken, B., 2015. Smoothing Parameter and Model Selection for General Smooth Models, vol. 111. Publications of the American Statistical Association, pp. 1548–1563.
Yang, Y., Russell, L.M., Lou, S., Hong, L., Guo, J., Ying, L., Singh, B., Ghan, S.J., 2017. Dust-wind interactions can intensify aerosol pollution over eastern China. Nat. Commun. 8.
Zender, C.S., Bian, H., Newman, D., 2003. Mineral dust entrainment and deposition (DEAD) model: description and 1990s dust climatology. J. Geophys. Res.: Atmos. 108.
Zhang, B., Jiao, L., Xu, G., Zhao, S., Tang, X., Zhou, Y., Gong, C., 2017. Influences of wind and precipitation on different-sized particulate matter concentrations (PM 2.5, PM 10, PM 2.5–10). Meteorol. Atmos. Phys. 1–10.
Zhang, H., Wang, Y., Park, T.W., Deng, Y., 2016. Quantifying the relationship between extreme air pollution events and extreme weather events. Atmos. Res. 188, 64–79.
Zhang, Q., Streets, D.G., Carmichael, G.R., He, K.B., Huo, H., Kannari, A., Klimont, Z., Park, I.S., Reddy, S., Fu, J.S., 2009. Asian emissions in 2006 for the NASA INTEX-B mission. Atmos. Chem. Phys. 9, 5131–5153.
Zhang, R., Wang, G., Guo, S., Zamora, M.L., Ying, Q., Lin, Y., Wang, W., Hu, M., Wang, Y., 2015. Formation of urban fine particulate matter. Chem. Rev. 115, 3803–3855.
Zhang, Z., Wang, X., Zhao, X., Liu, B., Yi, L., Zuo, L., Wen, Q., Liu, F., Xu, J., Hu, S., 2014. A 2010 update of National Land Use/Cover Database of China at 1:100000 scale using medium spatial resolution satellite images. Rem. Sens. Environ. 149, 142–154.